Engineering Structures 130 (2017) 67–82

Contents lists available at ScienceDirect

Engineering Structures

journal homepage: www.elsevier.com/locate/engstruct

Performance-based seismic design of self-centering steel frames with SMA-based braces

Can-Xing Qiu [a,b], Songye Zhu [b,*]

[a] Department of Civil Engineering, Shandong University, Jinan, Shandong Province, China
[b] Department of Civil and Environmental Engineering, The Hong Kong Polytechnic University, Hung Hom, Kowloon, Hong Kong

ARTICLE INFO

Article history:
Received 18 May 2015
Revised 23 September 2016
Accepted 24 September 2016

Keywords:
Performance-based seismic design
Performance-based plastic design
Self-centering
Steel braced frame
Shape memory alloy (SMA)
Superelasticity

ABSTRACT

This study proposes a performance-based seismic design (PBSD) method for steel braced frames with novel self-centering (SC) braces that utilize shape memory alloys (SMA) as a kernel component. Superelastic SMA cables can completely recover deformation upon unloading, dissipate energy without residual deformation, and provide SC capability to the frames. The presented PBSD method is essentially a modified version of the performance-based plastic design with extra consideration of some special features of SMA-based braced frames (SMABFs). Four six-story concentrically braced frames with SMA-based braces (SMABs) are designed as examples to illustrate the efficacy of the proposed design method. In particular, the variability in the hysteretic parameters of SMAs, such as the phase-transformation stiffness ratio and the energy dissipation factor, is considered in the PBSD method. Accordingly, four SMABFs are designed with different combinations of these hysteretic parameters. The seismic performance of the designed frames is examined at various seismic intensity levels. Results of nonlinear time-history analyses indicate that the four SMABFs can successfully achieve the prescribed performance objectives at three seismic hazard levels. The comparisons among the designed frames reveal that the SMABs with greater hysteretic parameters result in a more economical design in terms of the consumption of steel and SMA materials.

1. Introduction

Appropriately designed seismic-resisting structures are expected to respond satisfactorily to earthquakes without collapsing. However, they may still suffer from excessive permanent deformation, which may eventually lead to their demolition. For example, dozens of damaged reinforced concrete (RC) buildings were demolished because of large permanent inter-story drifts after the Michoacan earthquake in 1985 [1]. Recent investigations suggest that a residual inter-story drift ratio that exceeds 0.5% makes rebuilding a new structure more favorable than retrofitting or repairing a damaged structure [2]. Given that both the peak and residual deformation demands of structures are accentuated in modern earthquake engineering, various types of self-centering (SC) structural components and systems have been developed and studied in the past decades [3–13]. A popular means to implement SC structural systems is to combine a post-tensioned (PT) mechanism with energy dissipaters [3–12]. For example, Ricles et al. [4] proposed an innovative SC connection, in which PT strands ran through the frame width parallel with beams and were anchored at column flanges; bolted angles that connected beams and columns were used to dissipate energy. The test results showed that such SC connections demonstrated good energy dissipation capacity and experienced no residual deformation after a couple of inelastic cycles. Christopoulos et al. [7] developed an SC brace using PT aramid fibers, which underwent large axial deformation without structural damage and provided stable energy dissipation capacity.

Shape memory alloys (SMAs) comprise a class of metal alloys with appealing superelasticity and good energy dissipation [14–18]. After a number of preloading cycles (known as training treatment), SMAs can produces ideal flag-shape (FS) hysteresis without residual deformation [19]. Therefore, superelastic SMAs have gained increasing attention in the field of SC structural systems [20–37]. Dolce et al. [23] investigated the seismic performance of a scaled RC frame with SMA braces through shaking table tests, which showed that SMA braces greatly reduce the residual deformation of the RC frame. More studies can be found on SC steel frames with SMA-based braces (SMABs). For example, McCormick et al. [24] revealed the superiority of SMABs over conventional steel braces in limiting peak and residual inter-story drifts. Zhu

* Corresponding author.
E-mail address: ceszhu@polyu.edu.hk (S. Zhu).

http://dx.doi.org/10.1016/j.engstruct.2016.09.051
0141-0296/

and Zhang [25] developed SMABs that were used in a multistory braced frame, which successfully diminished post-earthquake residual deformation. In particular, the hysteretic behavior of SMABs can be adjusted by tuning their friction level and wire inclination [26]. Compared with a buckling-restrained braced frame (BRBF), the proposed SC braced frames can achieve a similar peak deformation demand but a considerably smaller residual interstory drift.

In contrast to extensive investigations on SC building structures, the corresponding seismic design methods of such structures have been rarely studied [38–41]. Recently, Kim and Christopoulos [38] proposed and validated a design procedure for PT SC moment-resisting frames (MRFs), in which the prescribed performance targets were set similarly to those of welded steel MRFs. Eatherton et al. [41] developed a design method for an SC rocking frame by focusing on controlling several performance limit states; single and dual frames were designed using their method, but seismic performance was not examined.

However, a rational design methodology for steel braced frames with SC SMABs has never been reported in literature. To fill in this knowledge gap, the current study proposes an ad hoc performance-based seismic design (PBSD) method for SC steel braced frames with SMABs. The performance-based plastic design method [42], which was previously developed for traditional steel moment and braced frames, is extended to the design of emerging seismic-resisting SMA-based braced frames (SMABFs), in which SC braces employed SMA cables that possess stable and repeatable cyclic properties after proper preloading (or training) treatment. At a constant temperature, a multistory SC steel frame with novel SMABs is designed as an example in consideration of the prescribed seismic performance targets. Different SMA cables may exhibit various transformation stiffness ratio and energy dissipation capacities depending on material properties, and the effect of such variability on seismic response has been noted [27]. Therefore, a generalized FS hysteresis, in which the variability in these two factors is particularly considered, is adopted in the proposed PBSD method, which offers the necessary flexibility to apply the PBSD method to steel frames with different types of SMABs. Moreover, the effect of potential high modes in seismic response of SMABFs is also considered during the design process. A systematic numerical assessment validates that steel SMABFs designed via the proposed method can achieve the prescribed seismic performance satisfactorily. Although this study is intended for multistory frames with SMABs, the proposed design framework can be further extended to other SC structures with FS hysteresis.

2. SMAB

Various configurations of SMABs have been developed, and they typically exhibit FS hysteretic behavior. Fig. 1(a) shows a representative configuration of the SMAB fabricated and tested by the authors at a room temperature in a laboratory. The brace is designed to be installed in a 1/4-scale two-story frame. The brace consists of two parts: (1) the core part, which is an SMA-based damper with an SC and energy-dissipation function, and (2) the extension parts, which are two steel tubes that extend the brace to a desired length. The mechanism of the SMA-based damper is shown in Fig. 1(b). This damper is composed of two steel blocks that slide against each other, two steel rods, and two bundles of Nitinol cables with the austenite finish temperature $A_f = -10$ °C. Axial displacement moves the steel rods in the slots of the steel blocks and stretches the SMA cables regardless of the damper being under tension or compression. Fig. 1(c) shows the cyclic testing result of the SMAB that has been properly trained before the formal test. The hysteretic behavior is associated with moderate energy dissipation and zero residual deformation upon unloading and can be idealized as a simple stabilized FS hysteresis, as shown in Fig. 1(c). Such FS idealization of the cyclic behavior of SMAs was commonly adopted in the previous studies [27–29]. A typical FS stress–strain relationship can be characterized by four parameters, namely, the initial modulus of elasticity E_{SMA}, "yield" stress σ_y, "post-yield" stiffness ratio α, and energy dissipation factor β. Notably, the Nitinol cables do not really yield in the cyclic test. In this case, "yield" refers to the yield-like stress plateau induced by the phase transformation of Nitinol. The parameters that correspond to Fig. 1(c) are $\alpha = 0.16$, $\beta = 0.5$, $\sigma_y = 465$ MPa, and $E_{SMA} = 46.5$ GPa, where σ_y and E_{SMA} are calculated based on the cross-sectional area and length of the Nitinol cables, respectively.

The Nitinol cables used in the tested brace may be replaced by a variety of other SMA cables with significantly different cyclic properties. The variability in FS hysteresis, particularly in two essential parameters (post-yield stiffness ratio α and energy dissipation factor β) should be considered in a design method if it is intended for different types of SMABs. Moreover, the deformation capacity of SMA cables also differs significantly. For example, the superelastic strain reaches up to 8% for Nitinol cables [14], 12% for Cu-Al-Mn SMA [20], 13.5% for FeNCATB SMA [43], and mono-crystalline Cu-Al-Be cables may exhibit superelastic strain of over 19% [18]. In addition, SMA-based damper is able to possess a very large superelastic capacity with a proper configuration [22]. Therefore, the proposed design in the current study assumes that SMAs' deformation does not exceed superelastic strain. Thus, the hardening behavior that may occur after the completion of superelastic phase transformation strain is not considered in this study. The adopted generalized FS hysteresis enables the extension of the proposed method to the design of other types of SC braced frames. It is noteworthy that the occurrence of hardening behavior and residual deformation at extremely large strain values may affect the seismic behavior of structures with SMA devices. Hardening behavior is generally beneficial to limiting structural displacement but tends to transfer a significant amount of force to adjacent structural members connected to braces. This phenomenon should be considered in design cases where SMA would likely deform under extremely large strain values. In addition, the FS hysteresis of SMAs is sensitive to ambient temperature, and the decreasing temperature that leads to a lower stress σ_y is often unfavorable in seismic response control. It should be noted that some types of SMAs are not suitable to low temperature applications [18]. Thus, SMABs are assumed to be applied in an indoor environment with stable room temperature and the effect of significant temperature variation is not considered in this study.

3. SC Single-Degree-of-Freedom (SDOF) system

The seismic behavior of structures is often dominated by structural fundamental modes. Nonlinear SDOF systems with FS hysteresis are systematically investigated under three suites of ground motions in this section.

3.1. Ground motions

Somerville et al. [44] developed three suites of ground motions that were generated for Los Angeles with exceedance probability of 50%, 10%, and 2% in 50 years. Each suite contains 20 records designated as LA01-LA20 (for design basis earthquakes, DBE), LA21-LA40 (for maximum considered earthquakes, MCE) and LA41-LA60 (for frequently occurred earthquakes, FOE). The 20 records were derived from ten historical records with frequency domain adjusted and amplitude scaled. The 20 earthquake records were modified from soil type S_B–S_C to soil type S_D. The 20 ground

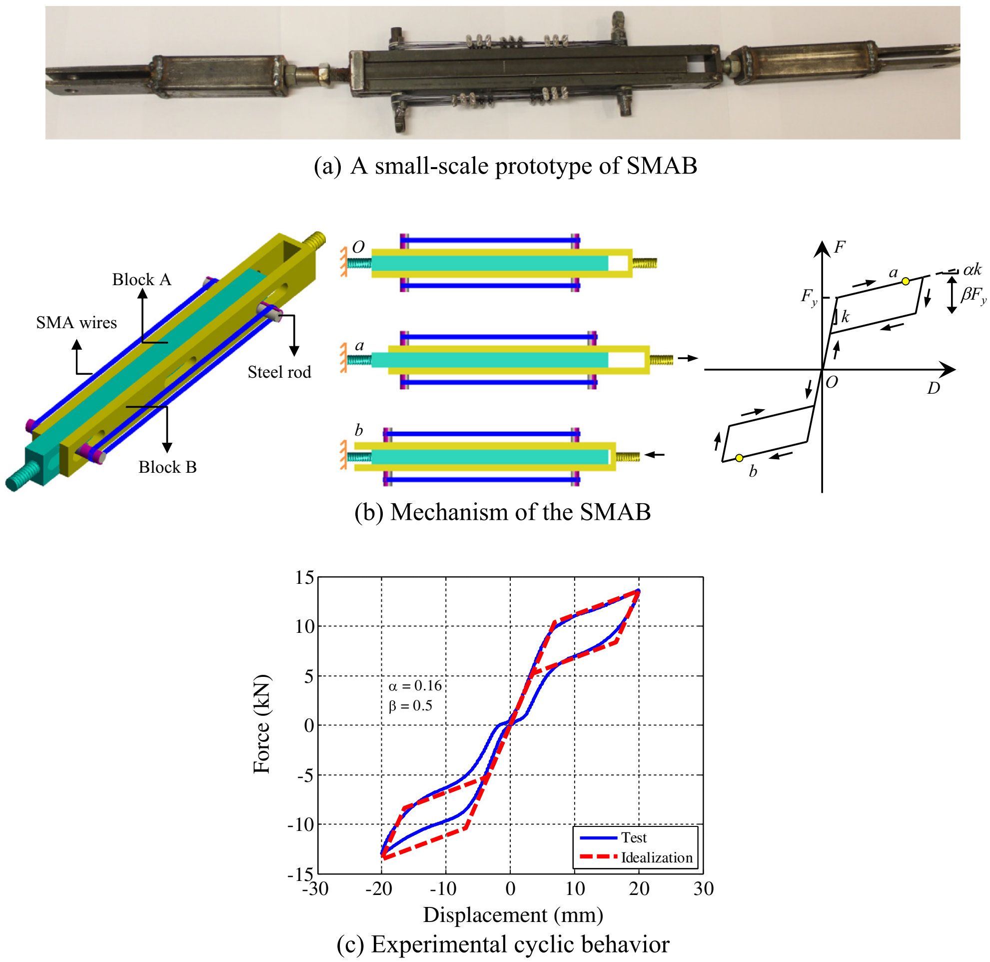

(a) A small-scale prototype of SMAB

(b) Mechanism of the SMAB

(c) Experimental cyclic behavior

Fig. 1. SMAB.

motions corresponding to DBE hazard level are used in the seismic analyses of SDOF systems, with the aim to develop the design framework. The seismic performance of the multistory frames is assessed by subjecting them to all three seismic hazard levels. Fig. 2 shows the 5%-damped elastic response spectra of the ground motions with an exceedance probability of 10% in 50 years. The geometric mean response spectrum of the 20 ground motions satisfactorily matches the design basis earthquake (DBE) spectrum, although great variability exists among the records.

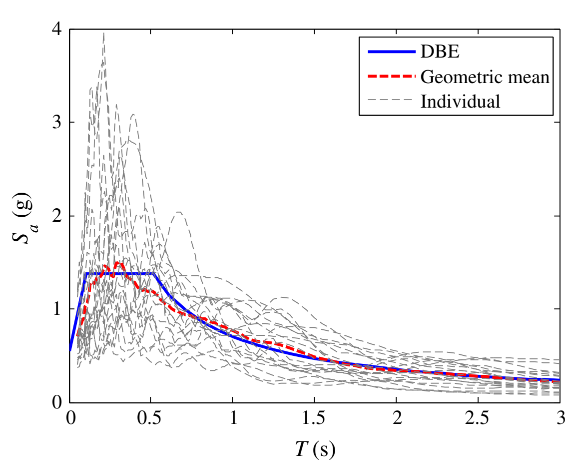

Fig. 2. Acceleration spectra of ground motion records.

3.2. μ-R-T Relationship

The seismic analyses of SC SDOF systems with varying FS hysteresis (as illustrated in Fig. 3) are presented in this section under the selected 20 DBE-level ground motions. The SDOF systems with varying elastic periods T and ductility ratios μ are analyzed, where the elastic periods T range from 0.1 s to 3.0 s at an interval of 0.1 s, and the ductility ratios μ are equal to 2, 4, 6, and 8. The ductility ratio, μ, is defined as the ratio of the peak deformation to the "yield" deformation (i.e., the deformation when the forward phase transformation stars). In particular, the hysteresis parameters α ranging from 0.0 to 0.20 and β ranging from 0.1 to 0.9 are consid-

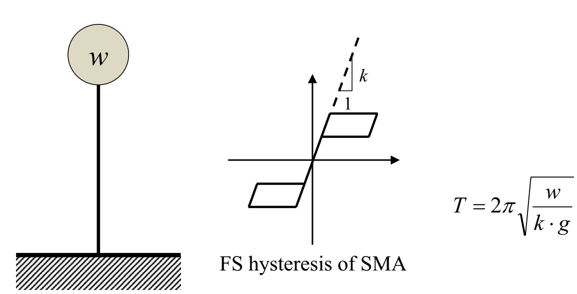

Fig. 3. Inelastic SC SDOF systems with FS hysteresis.

ered in the analyses. In real applications, these two parameters often exhibit large variability, because they are not only affected by SMA material properties, but also affected by the design of SMA-based devices. A similar range of α and β was also considered in a prior study [27]. Nonlinear constant-μ analyses of SC SDOF systems are performed, in which a constant ductility demand is initially prescribed and the corresponding strength reduction factor R, which is the ratio of the base shear of elastic SDOF to the yield force of the SC SDOF system, is subsequently searched by iteratively changing the yield point of SC SDOF systems. Such constant-μ analyses are performed for each ground motion. Consequently, for a specific μ value, the geometric mean of 20 different R values corresponding to 20 ground motions is computed. Then, the μ-R-T relationship of SDOF systems with FS hysteresis is constructed. Fig. 4 shows the μ-R-T relationships of four FS models with different α and β combinations, namely, ($\alpha = 0.04$, $\beta = 0.5$), ($\alpha = 0.04$, $\beta = 0.9$), ($\alpha = 0.16$, $\beta = 0.5$), and ($\alpha = 0.16$, $\beta = 0.9$). The third is to reproduce the cyclic behavior of the damper shown in Fig. 1. Compared with the first one, the second and third combinations represent cases with enhanced β and α levels, respectively, and the fourth combination represents the simultaneous increase of α and β. Large α and β values are generally beneficial to SC SDOF systems because they allow using large strength-reduction factors R. Therefore, the variability in hysteretic parameters α and β should be appropriately considered in designing SC structures. The following formula proposed by Seo [45] is adopted in this study to simulate the μ-R-T relationships shown in Fig. 4:

$$R = \mu^{\exp(a/T^b)}, \tag{1}$$

where a and b are the coefficients that depend on the aforementioned hysteretic parameters. Parameter a is usually negative. This empirical relationship is selected among various options because of the following reasons. (1) The formula has a clear physical implication: when $T \to 0$, $R \to 1$, and when $T \to \infty$, $R \to \mu$. (2) The influence of hysteretic parameters α and β can be conveniently incorporated into this formula. (3) The relationship is expressed using a relatively simple single formula. Through regression analyses based on Fig. 4, the following two coefficients are suggested:

$$a = -0.38 + 0.51\alpha + 0.16\beta, \tag{2a}$$

$$b = 0.31 - 0.05\alpha + 0.18\beta. \tag{2b}$$

The regression μ-R-T relationship can be obtained by substituting Eq. (2) into Eq. (1). Subsequently, the coefficient of determination R^2 is equal to 0.97 for Eq. (1), which indicates good fitness effect of this regression formula.

Fig. 4 compares the results of the numerical simulations and regression functions. Each curve in the figure represents a constant-μ curve. The adopted empirical formula agrees with the numerical simulation results well in all the cases shown in Fig. 4.

Given the estimated initial period T and the ductility target μ of the SDOF system, the required strength reduction factor R can be determined according to Eq. (1), and the design base shear v_y of the SDOF system is calculated as follows:

$$v_y = \frac{w \cdot S_a}{R \cdot g}, \tag{3}$$

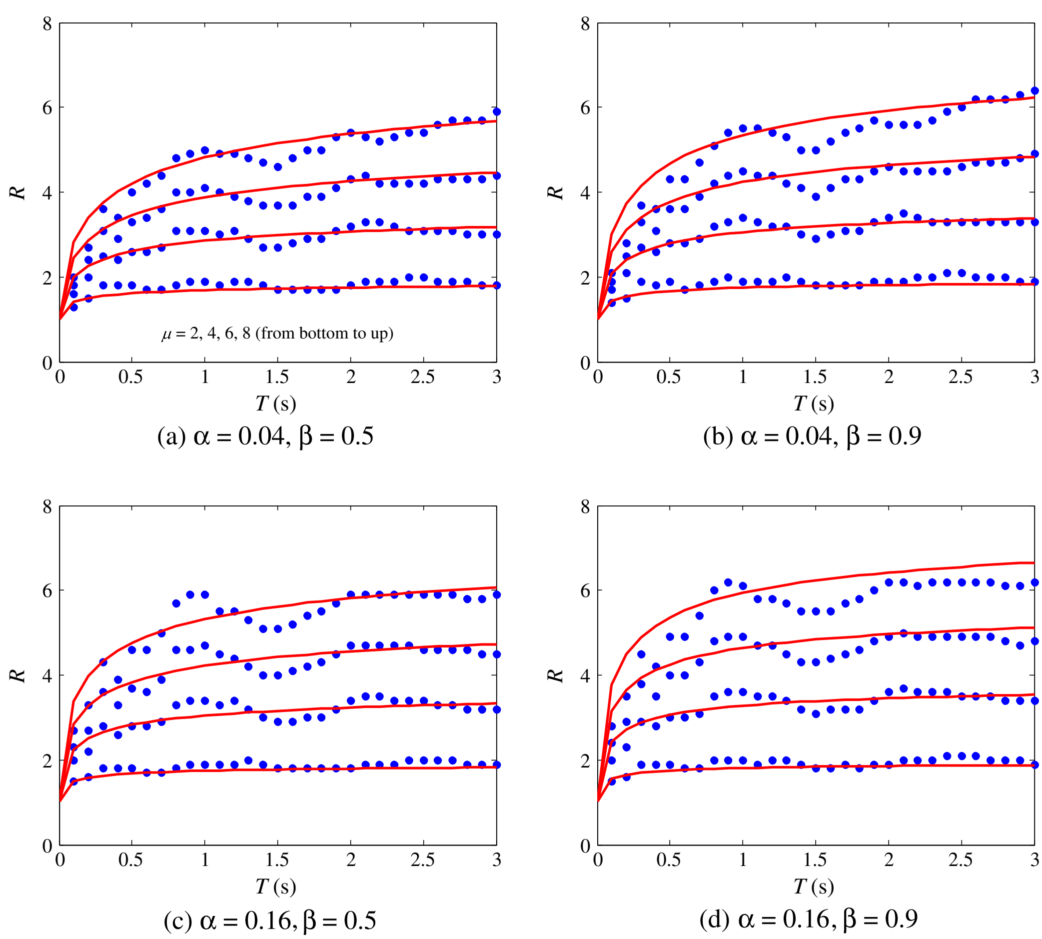

Fig. 4. μ-R-T relationships of SC SDOF (Dots: numerical simulation; Lines: fitting curves).

where w is the weight of the SDOF system, g is the gravity acceleration, and S_a is the spectral acceleration that corresponds to the natural period of the SDOF system.

3.3. Modified energy equivalent condition

Based on the energy balance concept [42,46], Lee et al. [47] proposed a modified energy equivalent equation as follows:

$$e_e + e_p = \gamma e_i, \tag{4}$$

where e_i is the peak strain energy of an elastic SDOF system; e_e and e_p represent the peak elastic and plastic strain energy, respectively, of a corresponding inelastic SDOF system with the same initial period T; and γ is a modification factor that depends on inelastic behavior. Lee et al. [47] proposed a simple estimation of γ based on the ductility demand for elasto-plastic behavior. However, the seismic analyses of the SC SDOF systems reveal that the modification factor is not only dependent on ductility demand μ and natural period T, but is also affected by hysteretic parameters α and β. Thus, a new estimation of factor γ is derived for the SC SDOF system in this study.

For two SDOF systems (one elastic and one inelastic) with the same initial stiffness k_e, Fig. 6 illustrates the energy equivalence concept in the form of peak base shear vs. peak displacement curves, in which v_y and δ_y refer to the yield force and the corresponding yield displacement, respectively, of the inelastic SDOF system. v_e and δ_e are the peak resisting force and displacement, respectively, of the corresponding elastic SDOF system. $\delta_u = \mu \cdot \delta_y$ represents the peak displacement of the inelastic SDOF system. Finally, α denotes the post-yield stiffness ratio. In the two SDOF systems, the three energy terms in Eq. (4) can be computed as follows:

$$e_e = \frac{1}{2} v_y \delta_y, \tag{5}$$

$$e_p = \frac{1}{2} v_y \delta_y (\mu - 1)[2 + \alpha(\mu - 1)], \tag{6}$$

$$e_i = \frac{1}{2} v_e \delta_e = \frac{1}{2} v_y \delta_y R^2. \tag{7}$$

Substituting Eqs. (5) to (7) into Eq. (4) provides the estimation of the energy modification factor γ as follows:

$$\gamma = \frac{\alpha(\mu-1)^2 + 2(\mu-1) + 1}{R^2} = \frac{\alpha(\mu-1)^2 + 2(\mu-1) + 1}{\mu^{2\exp[a/T^b]}}. \tag{8}$$

where the coefficients a and b are defined in Eq. (2). If the μ-R-T relationship developed in the last subsection for the SC SDOF system is substituted, then the energy modification factor can be expressed as a function $\gamma(\mu, T, \alpha, \beta)$ that considers the effects of the ductility demand μ, natural period T, and hysteretic parameters α and β of SC SDOF systems.

4. PBSD approach for SMABF

The emerging PBSD method is a probabilistic design framework that aims to realize the prescribed seismic performance of structures. Performance assessment is treated as a discrete Markov process that is described in a probabilistic form as follows [48]:

$$\lambda(DV) = \iiint G\langle DV|DM\rangle dG\langle DM|EDP\rangle dG\langle EDP|IM\rangle d\lambda(IM), \tag{9}$$

where IM is the intensity measure that is commonly represented by the 5%-damped spectral acceleration at the fundamental period, i.e. $S_a(T_1, 5\%)$; EDP denotes engineering demand parameters such as peak inter-story drift ratios and floor accelerations; DM is a damage measure that refers to the damage extent of both structural and non-structural components; and DV is the decision variable that includes building cost, dollar losses, downtime, and casualty risks, among others. Given that DM is closely related to EDP, DM may be directly represented by EDP.

In this study, the performance-based plastic design method [42], which is one of the well-known PBSD methods, is modified for SMA-based SC structural systems. This PBSD method has been successfully applied in the design of various structural systems. However, this study is the first attempt to extend this method to the design of seismic-resisting SC frames with SMABs.

4.1. Performance-based plastic design method

The performance-based plastic design procedure was firstly proposed by Leelataviwat et al. [42]. It was originated from the energy equivalence concept through an investigation of an elastic and perfectly plastic structural system [46]. Since then, the performance-based plastic design method has been successfully applied to the seismic designs of steel moment frames [47], concentrically braced frames [49], eccentrically braced frames [50], truss moment frames [51], buckling-restrained braced frames [52], and buckling-restrained knee-braced truss moment frames [53]. The key concept in the performance-based plastic design remains to be the modified energy equivalent condition [47]. When applied to multi-story frames, the modified energy equivalent condition is expressed as follows:

$$E_e + E_p = \gamma E_i, \tag{10}$$

where E_e and E_p denote the peak elastic and plastic strain energy, respectively, of an inelastic multi-degree-of-freedom (MDOF) structure; E_i is the peak elastic strain energy of a corresponding elastic MDOF structure with the same elastic periods; and γ indicates the energy modification factor.

When a structure behaves elastically, the peak strain energy can be approximated by the seismic input energy as follows [46]:

$$E_i = \frac{1}{2}\frac{W}{g} S_v^2 = \frac{1}{2}\frac{W}{g}\left(\frac{S_a T}{2\pi}\right)^2, \tag{11}$$

where W is the total building weight; T is the fundamental period of the structural system; and S_v and S_a are the pseudo-velocity and pseudo-acceleration spectra, respectively. The total building weight W, instead of the first modal weight, is used in Eq. (11) to account for multiple vibration modes. The estimation shown in Eq. (11) is based on the assumption that the pseudo-velocity spectra for different vibration modes are nearly constant and can be represented by the spectral value corresponding to the fundamental period $S_v(T)$.

In an inelastic structure, Akiyama [54] approximated elastic vibrational energy by reducing the MDOF structure into an SDOF system with a weight W:

$$E_e = \frac{1}{2}\frac{W}{g}\left(\frac{V_y g}{W}\frac{T}{2\pi}\right)^2 = \frac{WT^2 g}{2\pi^2}\left(\frac{V_y}{W}\right)^2, \tag{12}$$

which implies that the relationship between the yielding base shear V_y and the corresponding pseudo-acceleration A_y is

$$V_y = \frac{W}{g} A_y, \tag{13}$$

The preceding equation is accurate for an SDOF system; however, it only functions as an approximation that may slightly underestimate pseudo-acceleration for an MDOF structure [55]. The plastic energy E_p of an inelastic multistory frame can be computed based on the lateral seismic force and plastic floor displacement of each floor. Compared with [47], the computation of E_p in this study particularly considers the favorable effect of the "post-yield" stiffness ratio α in a form similar to that of Eq. (6), as follows:

$$E_p = \frac{1}{2}\left(\sum_{i=1}^{n} F_i h_i \theta_p\right)[2 + \alpha(\mu - 1)], \tag{14}$$

where n is the number of floors, h_i is the height of the ith floor from the base, F_i is the lateral seismic force on the ith floor, and θ_p is the plastic roof drift ratio. The variables can be expressed respectively as

$$F_i = C_i \cdot V_y, \tag{15}$$
$$\theta_p = (\mu - 1)\theta_y, \tag{16}$$

where C_i is the lateral force coefficient on the ith floor, and θ_y is the roof drift ratio that corresponds to the yield base shear force.

If the energy modification factor γ derived for the SC SDOF system is used for MDOF structures, the design base shear can be determined by solving Eq. (10) after substituting Eqs. (8), (11), (12), and (14), as follows:

$$V_y/W = \left(-\lambda + \sqrt{\lambda^2 + 4\gamma S_a^2}\right)\Big/2, \tag{17}$$
$$\lambda = \left[1 + \frac{\alpha(\mu - 1)}{2}\right]\left(\frac{8\pi^2}{T^2 g}\right)\left(\sum_{i=1}^{n} C_i h_i\right)\theta_p. \tag{18}$$

Eq. (17) determines the design base shear of a multistory steel frame. If a single-story steel frame is of interest, the design base shear can be determined by a simpler formula, that is, Eq. (3). Notably, knowledge on the structural fundamental period T, which is often unknown at the beginning of a design, is required in determining design base shear. In practice, the structural fundamental period T can be initially evaluated according to empirical relations in ASCE 7-10 [56] or according to elastic or inelastic displacement spectrum using direct displacement-based method [39]. Iteratively adjusting T may be necessary after the initial design. Moreover, some parts of the derivation are based on the simplified SDOF assumption. Thus, Eq. (17) only offers a reasonable approximation of the design base shear of an inelastic structure.

Eq. (17) also enables the consideration of different lateral force distributions, which is discussed in the following subsection. Given that Eqs. (8) and (14) are used, determining design base shear appropriately accounts for the effects of hysteretic parameters α and β, which is essential in designing SMABFs. Fig. 5 plots the minimum normalized design base shear V_y/W as a function of α and β by assuming T = 1.2 s and μ = 5. The selected T and μ are consistent with the design example of the six-story braced frame presented in Section 5. A large α or β corresponds to small design base shear forces. When β = 0.5, increasing α from 0 to 0.2 reduces the normalized design base shear from 0.216 to 0.174, which corresponds to a decrease of approximately 20%. When α = 0, increasing β from 0.1 to 0.9 reduces the normalized design base shear from 0.246 to 0.188, which corresponds to a decrease of approximately 24%. Thus, increasing α or β has comparable benefits in reducing design base shear. Reduction reaches up to 39% when α and β are simultaneously increased from 0 to 0.2 and from 0.1 to 0.9, respectively.

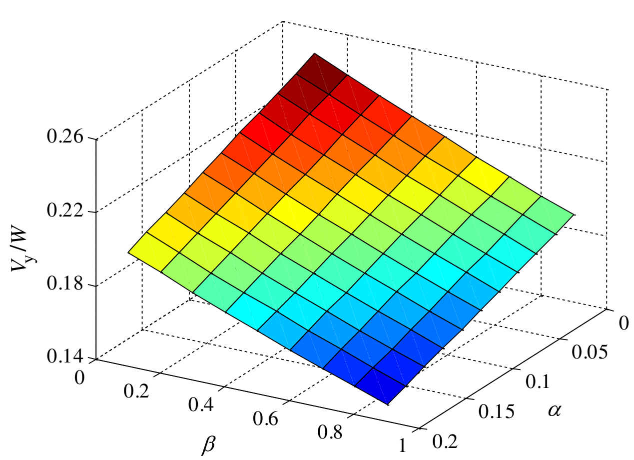

Fig. 5. Relationship between design base shear and properties of SMABF (T = 1.2 s and μ = 5).

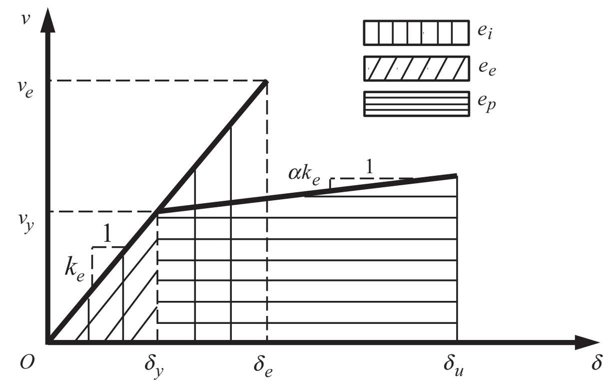

Fig. 6. Energy equivalence concept in PBSD method.

4.2. Lateral force pattern

The nonlinear dynamic analyses in a previous study [57] show that the seismic behavior of SC steel braced frames may exhibit a noticeable high-mode effect. Consequently, the high-mode effect tends to result in the concentration of the maximum inter-story drift ratio in the upper stories. To mitigate the high-mode effect in seismic response of SMABFs, a modified lateral force pattern proposed by Chao et al. [58] is used in this study instead of the conventional pattern defined in ASCE 7-10 [56]. The modified lateral force pattern is defined as

$$C_i = (p_i - p_{i+1})\left(\frac{w_n h_n}{\sum_{j=1}^{n} w_j h_j}\right)^{qT^{-0.2}}, \tag{19}$$

$$p_i = \left(\frac{\sum_{j=i}^{n} w_j h_j}{w_n h_n}\right)^{qT^{-0.2}}, \tag{20}$$

where w_j and h_j are the floor weight and floor height of the jth floor, respectively; and q affects the lateral force distribution along the building height and may vary with different structural systems. The lateral force distribution factors are normalized to obtain $\sum_{i=1}^{n} C_i = 1$.

Fig. 7 shows a direct comparison between the ASCE-compliant force pattern and the modified lateral force patterns with q equal to 0.50 and 0.75, respectively, for the six-story frame described in the next section. Compared with ASCE 7-10 [56], the force patterns adopted in this study allocate greater forces on top of a building. The seismic force acting on the roof is increased by approximately 67% and 23% when q is equal to 0.50 and 0.75, respectively. Such a large force on the top strengthens brace design in the upper stories. As suggested in a previous study [58], a q value equal to 0.75 is adopted to consider the high mode-induced concentration of the maximum inter-story drift in the top stories.

4.3. Design of SMABs

The design shear force in each story can be determined with the lateral force distribution along the building height, and thus, the

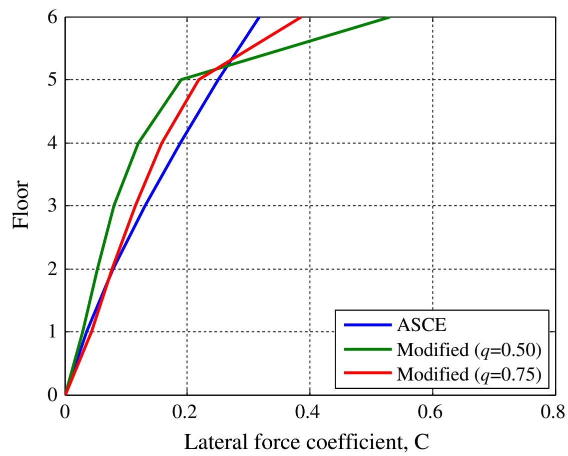

Fig. 7. Different lateral force patterns (T = 1.2 s).

bracing elements that resist the lateral forces can be designed accordingly. The design of SMABs depends on bracing configurations. If an inverted V-bracing configuration is utilized, then the cross-section area A_i and length l_i of the SMA cables in one brace in the ith story are given respectively by

$$A_i = \frac{\sum_{j=i}^{n} C_j V_y}{2\cos\theta_i \cdot \sigma_y}, \tag{21}$$

$$l_i = \frac{E_{SMA}\theta_y(h_i - h_{i-1})\cos\theta_i}{\sigma_y}, \quad h_0 = 0, \tag{22}$$

where E_{SMA} and σ_y are the elastic modulus and "yield" stress of the SMA cables, respectively; and θ_i is the inclination angle of the brace in the ith story. Notably the "yield" stress σ_y of SMAs is sensitive to temperature, and σ_y corresponding to the lowest temperature should be used in Eq. (21) if SMABs are used in an environment with temperature variation. However, some types of SMAs are not suitable for such applications with great temperature fluctuation (particularly at cold temperature). Therefore, the design examples presented in this study only consider the application of SMABs in an indoor environment with relatively stable room temperature.

4.4. Design of frame members

The beam and column members of SMABFs can be designed in a manner similar to that of BRBFs according to the AISC provisions [59]. To avoid potential overloading, the adjusted brace strength should be used in the frame member design as follows:

$$P = \phi\omega R_y F_y, \tag{23}$$

where F_y is the yield strength of braces; the overstrength factor R_y, resistant factor ϕ, and strain hardening adjustment factor ω are set as 1.1, 0.9, and 1.5, respectively. The strain hardening adjustment factor ω accounts for the increased brace force induced by the nontrivial post-yield stiffness ratio α. However, some superelastic SMAs (e.g., Nitinol) may experience highly apparent strain hardening after the completion of stress-induced phase transformation; a higher ω factor should be set if such strain hardening behavior is expected to occur. The SMA cables in the configuration shown in Fig. 1 are stretched when the brace is subjected to either tension or compression. Consequently, the compressive and tensile strengths of the brace remain nearly the same, and thus, compression strength adjustment is unnecessary. If the beam-to-column connections are designed as hinge connections, then bending moments in the frame members are minimized, and frame columns and beams can be designed to mainly carry axial loads.

4.5. Step-by-step design procedure

The flowchart of the proposed design method for a multistory SMABF is provided in Fig. 8. The design procedure is outlined as follows.

1. Specify the design parameters of the SMABF, such as the total number of stories n, story height h_i, number of braced bays, and tributary weight w_i in each floor level.
2. Characterize the "post-yield" stiffness ratio α and energy dissipation factor β of the selected SMA materials.
3. Specify the performance objectives, and determine the corresponding controlled *EDP*, such as the peak inter-story drift ratio θ_u and ductility demand μ.
4. Estimate the fundamental period T of the braced frame according to some empirical formula (e.g., ASCE 7-10 [56]) or according to elastic or inelastic displacement spectrum using direct displacement-based method [39]. The iterative adjustment of T may be necessary until the selected T converges to the final design value.
5. Calculate the yield inter-story drift ratio by $\theta_y = \theta_u/\mu$, and the inelastic inter-story drift ratio by $\theta_p = \theta_u - \theta_y$.
6. Determine the lateral force pattern C_i according to Eq. (19), which considers a high-mode effect.
7. Determine the strength reduction factor R of the SDOF system by substituting T, μ, α, and β into Eq. (1).
8. Determine λ by substituting θ_p, μ, α, and C_i into Eq. (18), and determine γ subsequently according to Eq. (8).
9. Determine the design base shear V_y by substituting λ, γ, S_a, and W into Eq. (17).
10. Determine the lateral force F_i on each floor according to Eq. (15).
11. Design the SMABs, including the determination of cross-section area and length of the SMA cables according to Eqs. (21) and (22), respectively.
12. Design column and beam members based on the adjusted brace strength.
13. Check the fundamental period T of the frame, and adjust the design if the actual T is far from the initial assumption in Step 4.
14. Evaluate structural seismic performance, and adjust the design if the seismic performance fails to satisfy the performance objectives. For example, the design base shear V_y and the lateral force pattern C_i can be modified.

5. Design example of SMABF

5.1. Building model

A six-story braced frame that has been used in a number of previous studies (e.g., [26,52,60] is adopted in this study. Fig. 10 shows the plan and elevation layouts of the prototype structure. The steel frame has a chevron-braced configuration. The bay width is 9.14 m, and the story height is 5.49 m for the first story and 3.96 m for the other stories. Six braced bays are used in one direction to resist lateral seismic force. The seismic tributary mass for the one-bay braced frame is 1/6 of the total floor mass. ASTM A992 steel is used for the beam and column members. The original braced frame (denoted as 6vb2) was designed by Sabelli et al. [60] according to NEHRP [61]. The frame was expected to be located in downtown Los Angeles. Additional structural details can be found in [60]. The original design employed a response modification factor of 8 and an occupancy importance factor of 1.

This six-story frame, including the braces, beams, and columns, is redesigned as several SMABFs using the PBSD method presented

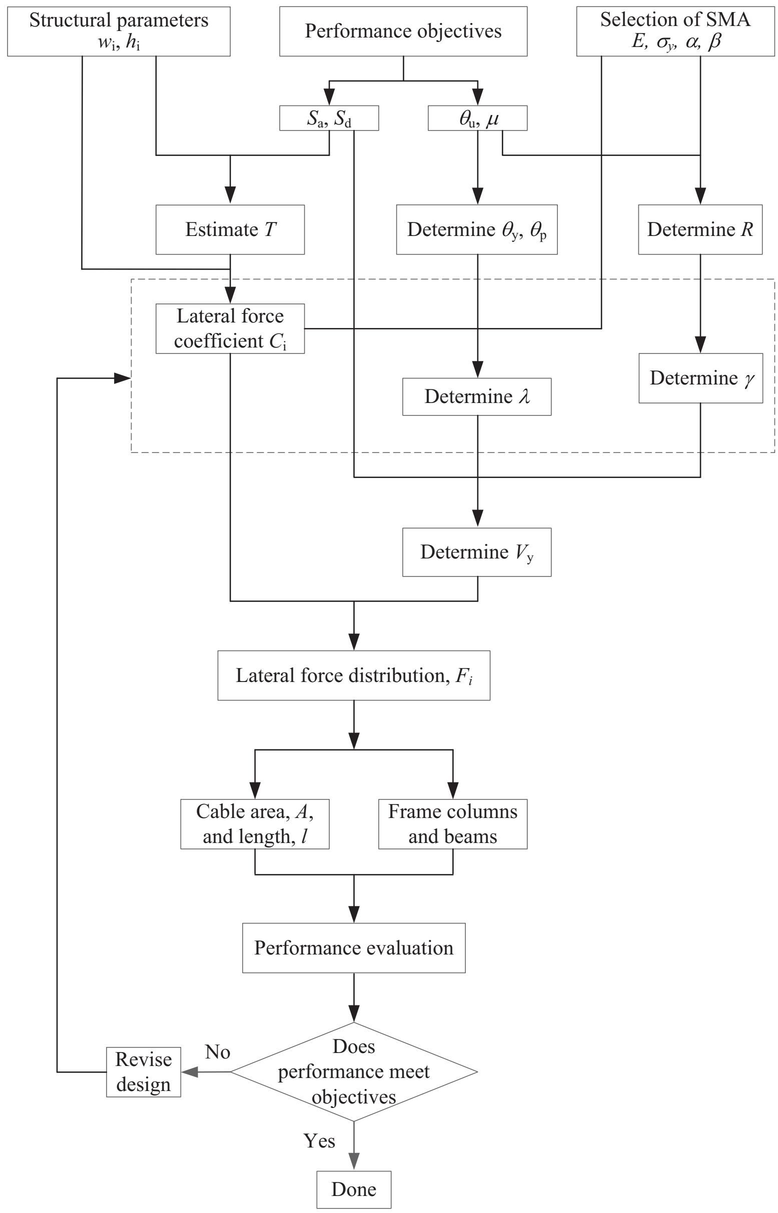

Fig. 8. Design flowchart of SMABF.

in the last section. All the SMABFs are assumed to be located in an indoor environment with relatively stable room temperature. Thus the impact of ambient temperature change need not be considered. Moreover, all beam-to-column connections in the original design are modified as hinge connections in this study because the latter can eliminate connection moment and accommodate large rotation without damage [62]. Fig. 10(b) shows a close-up view of the beam-to-column connection suggested by Fahnestock et al. [62].

5.2. Seismic performance targets

The modern PBSD should properly consider structural and non-structural damages. Given the excellent superelasticity of SMAs and the hinge design of beam-to-column connections, the designed SMABFs are expected to bear a large lateral deformation without significant damage. Among many damage measure indices, the peak inter-story drift ratio is often regarded as the most straightforward option. However, the limits of inter-story drift ratios that correspond to damage levels vary among different design specifications. For example, ASCE 41-06 [63] presents a wide range of inter-story drift ratios from 1% to 2% for various non-structural components at the DBE hazard level. The Vision 2000 report [64] defines three performance targets that correspond to three seismic hazard levels in consideration of structural and non-structural damages (i.e., 0.5%, 1.5%, and 2.5% at the FOE, DBE, and MCE hazard levels, respectively). The report [64] recommends the post-earthquake residual inter-story drift ratios to be negligible, 0.5%, and 2.5% at the FOE, DBE, and MCE levels, respectively. Thus, this study adopts the similar peak inter-story drift targets of 0.5% and 2.5% for the FOE and DBE levels, respectively. However, the inter-story drift limit proposed in the literature for the MCE hazard level becomes too conservative for the proposed SMABF with hinge connection design. The hinge connection design shown in Fig. 10(b) enables to withstand an inter-story drift ratio of 4.8% with only minor yielding [62]. Therefore, an inter-story drift ratio of 4.0% is selected as the design target at the MCE hazard level.

The target demands of brace ductility needs to consider deformation capacity of SMA materials. For example, the superelastic strain of Nitinol is up to 8%; whereas monocrystalline Cu-Al-Be exhibits a considerably greater deformation capacity. In the present study, the ductility demands of SMABs are set as 1.7, 5.0, and 12.0 at the FOE, DBE, and MCE seismic hazard levels, respectively. The inter-story drift ratio undergoes the same ductility as SMABs. According to these ductility demands, the yield inter-story drift ratio is estimated to be $\theta_y = 0.3\%$.

Seismic damage in different types of non-structural components can be deformation- or acceleration-sensitive. In addition to the peak and residual inter-story drift ratios, floor accelerations should also be assessed. However, the acceleration limits for different non-structural components vary significantly [63]. In this study, the limits for peak floor accelerations are assumed as 0.5, 1.0, and 1.5 g at the FOE, DBE, and MCE levels, respectively.

Fig. 9 summarizes the performance targets at three seismic hazard levels. It should be noted that the current performance targets are set as sample illustrations. Designers or stakeholders can decide different performance targets if desired.

5.3. Building design

The presented PBSD method does not obtain the design base shear by directly using the response modification factor but implicitly considers the μ-R-T relationship when computing the energy modification factor of input energy. Moreover, the ASCE 7-10 [56] code uses the equivalent lateral force design method; whereas the PBSD method is based on a prescribed displacement or deformation targets, which will reduce iteration loops. In this study, different SC structures designed with various design base shears are expected to achieve the same performance objectives as long as the design base shears are determined from the V_y/W-α-β surface.

The original six-story frame is redesigned as six-story SMABFs using the design procedure presented in Section 4.3 and outlined in Fig. 8. Performance targets are specified at three hazard levels. The braced frames can be designed according to the performance targets at any level or even three levels simultaneously as long as the corresponding seismic spectrum is used. In this case study, the SMABFs are initially designed according to the performance targets (including peak inter-story drift ratio and ductility demand) at the DBE level. The seismic performance of the designed frames is then assessed at the FOE and MCE levels.

Given that the developed PBSD approach enables the consideration of the variability in hysteretic parameters α and β of SMABs, four frames with different combinations of α and β parameters are designed to examine the efficacy of the developed PBSD approach. The four frames are denoted as S1 to S4 (Table 1) and designed to satisfy the same performance targets. Structure S3 employs SMABs with smaller values for hysteretic parameters α and β. Compared with S3, Structures S1 and S4 correspond to enhanced α and β parameters, respectively. Structure S2 employs braces with simultaneously enhanced α and β parameters. Among them, the parameters in Structure S1 are consistent with the brace testing results shown in Fig. 1.

Table 1 summarizes the building information of the four designed frames, including the initial design information, the design base shear, the fundamental period, and the information of SMABs and frame members. Table 1 enables direct examination of the influences of the hysteretic parameters on the final design of steel braced frames. As shown in Fig. 5, the variation in hysteretic parameters α and β leads to the distinct change in design base shear. Among the four cases, S3 and S2 are associated with the highest and lowest design base shears, respectively, whereas S1 and S4 exhibit an intermediate design base shear. Consequently, the final designs of S3 and S2 consume the most and least amount of steel, respectively. S1 and S4 use similar amounts of steel. Moreover, design base shear determines the lateral force distribution along the building height, and the lateral forces subsequently determine the cross-section areas of the SMA cables in the braces. However, the length of the SMA cables in the braces is determined by the yielding inter-story drift ratio θ_y. Thus, all four frames use the same cable lengths: 1.05 m in the first story and 0.90 m in the other stories. Compared with S3, Structures S1 and S4 reduce the material consumption of steel and SMA by approximately 4% and 13%, respectively. Structure S2 reduces steel and SMA consumption by 15% and 25%, respectively. These results indicate that using SMABs with greater α and β values in the design is favorable and cost-effective.

The fundamental period of the six-story frames is initially estimated according to the displacement target. According to the displacement-based design method [39], the target roof displacement of the frame is transformed to the target displacement of an equivalent SDOF, and then structural fundamental period can be estimated from elastic or inelastic displacement spectrum. The initial estimation of the fundamental period is approximately 1.20 s, which is only slightly shorter than those of the final designs of the frames ranging 1.22 s to 1.39 s. Therefore, no iterative adjustment of the fundamental period is performed in the design.

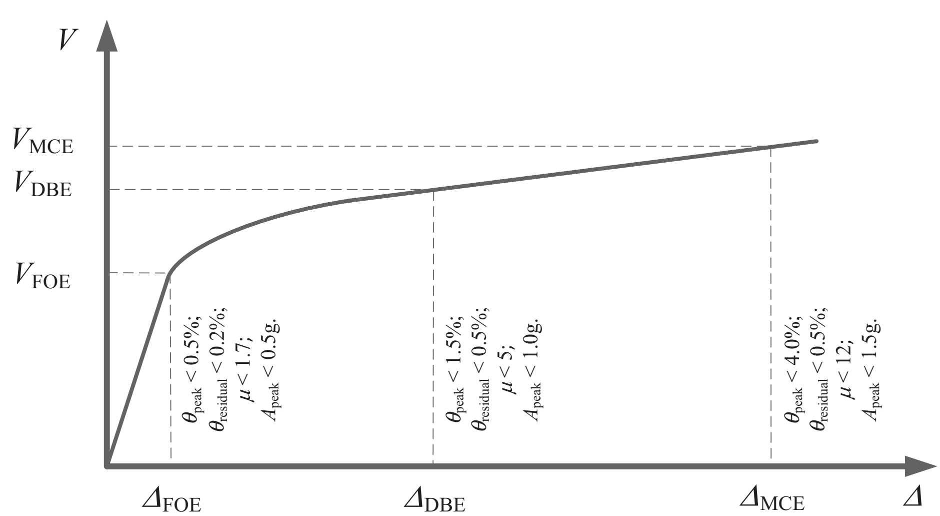

Fig. 9. Performance targets at three discrete seismic hazard levels.

Table 1
Building design information.

Structures		S1	S2	S3	S4
α		0.16	0.16	0.04	0.04
β		0.5	0.9	0.5	0.9
V_y/W		0.140	0.120	0.161	0.139
T (s)		1.29	1.39	1.22	1.29
Sectional area of SMA cable in a brace (mm^2)	6th story	743.7	637.1	848.6	734.7
	5th story	1166.4	999.3	1330.9	1152.2
	4th story	1472.4	1261.5	1680.2	1454.6
	3rd story	1693.6	1451.0	1932.6	1673.1
	2nd story	1843.4	1579.3	2103.5	1821.1
	1st story	2276.3	1950.2	2597.5	2248.7
Length of SMA cable (m)	Other stories	0.90	0.90	0.90	0.90
	1st story	1.05	1.05	1.05	1.05
Volume of SMA (cm^3)		17,229	14,760	19,660	17,020
Column sections	4th–6th story	W14 × 53	W14 × 48	W14 × 53	W14 × 53
	1st–3rd story	W14 × 132	W14 × 120	W14 × 132	W14 × 132
Beam sections	4th–6th story	W14 × 30	W14 × 26	W14 × 34	W14 × 30
	1st–3rd story	W14 × 38	W14 × 30	W14 × 43	W14 × 38
Steel weight (ton)		9.9	8.8	10.3	9.9

5.4. Seismic performance assessment

To evaluate the seismic performance of the designed frames, their numerical models are built using the computer program OpenSees [65]. Only one braced bay is modeled in each case, as shown in Fig. 10(c). The beams and columns are modeled with force-based beam–column elements. Previous studies [66] have demonstrated the advantages of force-based beam–column elements over displacement-based elements. The columns are continuous and fixed at their bases. The beam-to-column connections in the braced bay are modeled as hinged connections. ASTM A992 steel is used for the beam and column elements. No strength or stiffness deterioration due to local buckling or low cycle fatigue is assumed to the beam and column elements. Each brace is modeled as an element whose cross section at each integration point is an assembly of uniaxial fibers. SMA cables are modeled using the *SelfCentering* material. It is assumed that SMA cables are properly treated through cyclic training before their formal use and thus do not exhibit residual deformation upon unloading.

The effective seismic mass for a one-bay braced frame is 1/6 of the total floor mass. The tributary floor mass is acting on one leaning column, as shown in Fig. 10(c). The leaning column is assumed to have the same displacement as the braced bay at each floor level. Although the leaning column has a large cross section, the leaning columns in the two adjacent stories are connected by a hinge. Consequently, the leaning column does not contribute any lateral stiffness or strength to the entire structure. The gravity load is borne by the leaning column, whereas lateral seismic forces are resisted by the braced frame. The leaning column also accounts for the P-Δ effect during the dynamic simulation. Apart from vertical gravity loads, the one-bay braced frame is also subjected to horizontal seismic ground motions at the base. Only the in-plane seismic vibration of the frame is studied, whereas torsional response around a vertical axis is not considered.

Nonlinear time-history analyses are conducted to assess the seismic performance of the four designed SMABFs at three seismic intensity levels. The three suites of ground motions described in Section 3.1 are also employed in the dynamic simulations. The

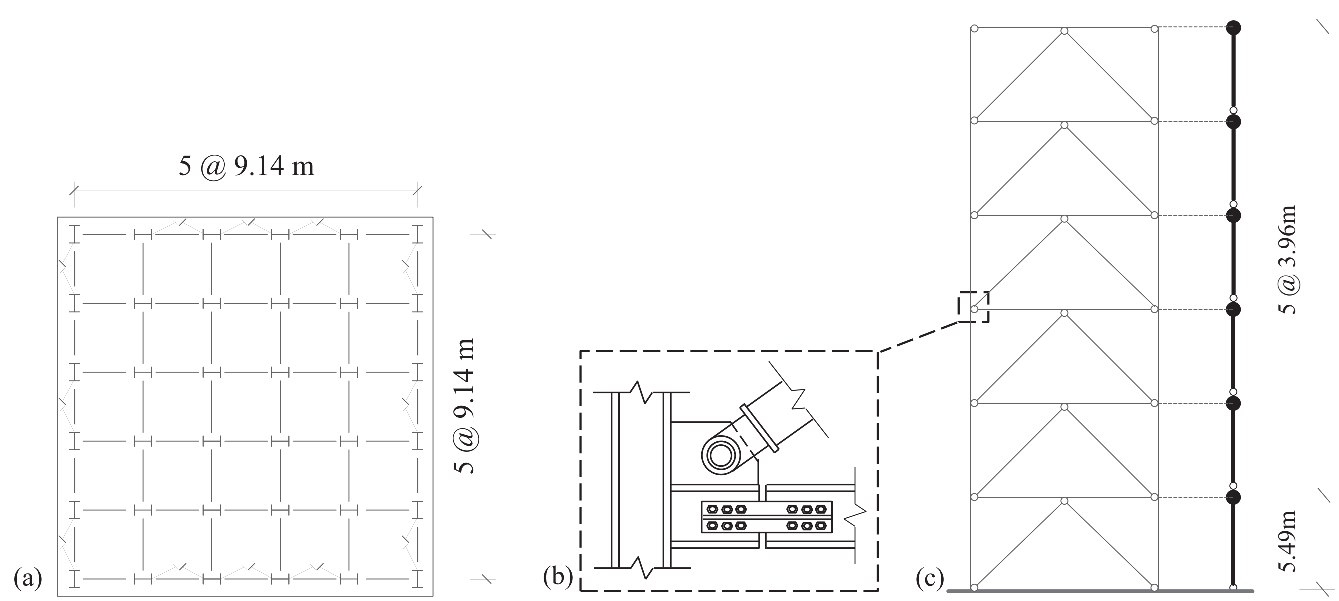

Fig. 10. Prototype 6-story frame building with SMAB: (a) plan layout; (b) brace-to-frame and beam-to-column connections; (c) elevation view.

durations of dynamic simulations are sufficiently long, and thus, free vibration decays and structural residual deformation can be accurately measured. The evaluated performance indices include the peak inter-story drift ratio, residual inter-story drift ratio, peak floor acceleration, and peak ductility demand of the SMABs, where the inter-story drift ratio is defined as the ratio of the relative displacement between two adjacent floors to the corresponding story height. The ductility demand is defined as the ratio of peak displacement to "yield" displacement. The geometric mean values of the responses under 20 ground motions are calculated to represent the average response.

Fig. 11 presents the results of the peak inter-story drift ratios and brace ductility demands of Frame S1 under FOE, DBE, and MCE seismic ground motions. Apparent record-to-record deviations exist among the results, and thus only the geometric mean of the 20 values is plotted. Since the frame is directly designed according to the DBE spectrum and the corresponding performance targets, the seismic performance at the DBE level is first examined. Fig. 11(c–d) show that the designed frame can satisfy the performance targets in terms of peak inter-story drift ratios and peak ductility at the DBE hazard level. The maximum inter-story drift demand at the DBE level occurs in the top story and is equal to 1.48%. The minimum response occurs in the first story, mainly because of the contribution of the fixed column bases. In general, the geometric mean inter-story drift ratios are distributed uniformly along the building height. Similar observations can be made for the brace ductility demand. Since the SMABs are major seismic-resisting components, the brace ductility demands are essentially the same as the ductility demand of inter-story drift. Compared with the performance targets, the brace design is slightly conservative in terms of ductility demand, because the designed structure yields a bit later than expected due to the influence of fixed column bases. Another similar SMABF is also designed using the vertical distribution pattern of seismic forces defined in ASCE 7 code (as

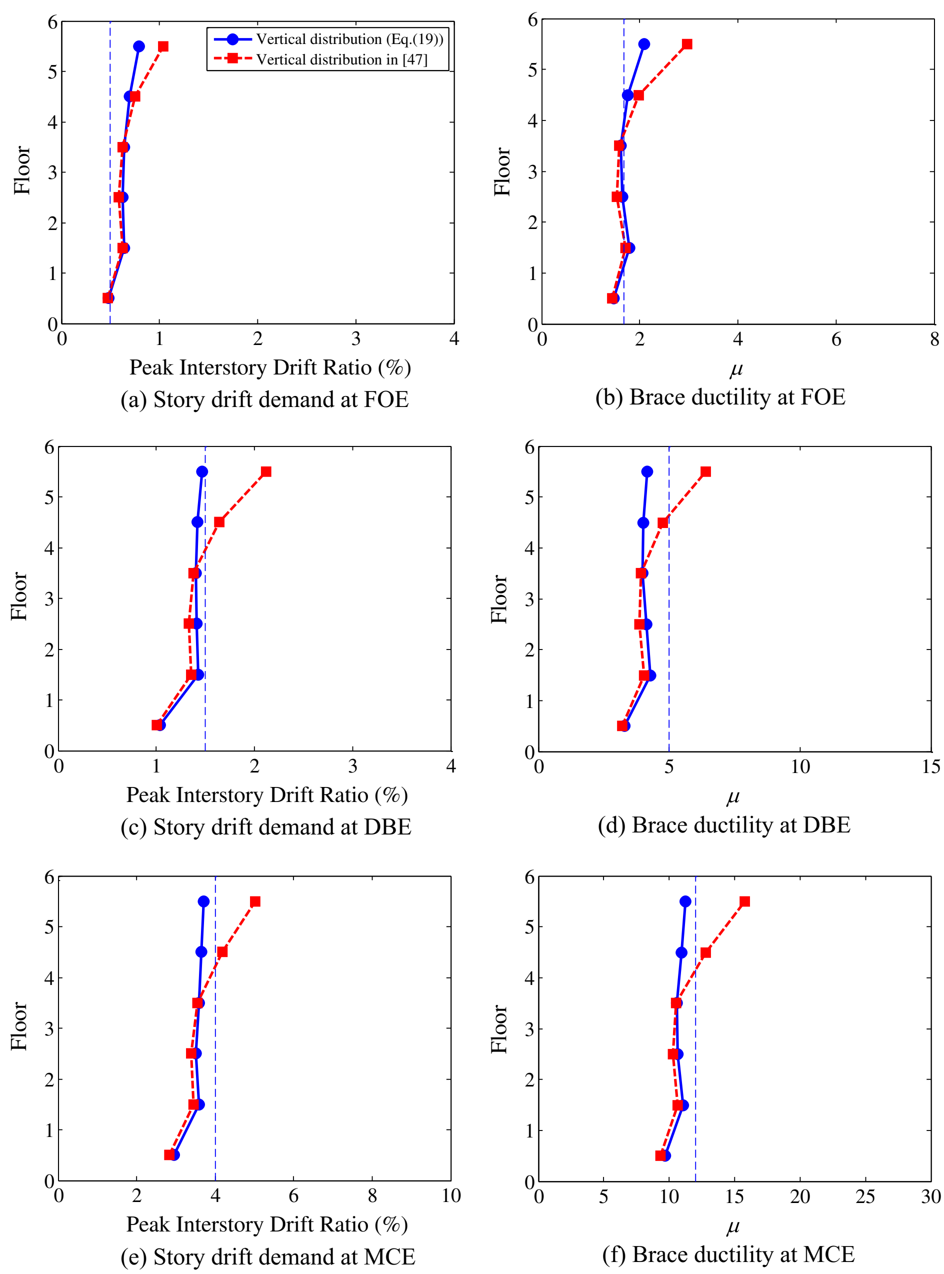

Fig. 11. Seismic performance of Structure S1 at three hazard levels.

shown in Fig. 7). The geometric mean responses of the frame designed with the code-compliant lateral force pattern are also shown in Fig. 11. The deformation concentration in the upper two stories demonstrates a noticeable high-mode effect. As a result, the seismic performance of the counterpart frame considerably exceeds the design targets. This comparison clearly illustrates the benefit of the modified lateral force pattern presented in Section 4.2 in the PBSD procedure.

Fig. 11(a–b) and (e–f) show the peak inter-story drift ratios and brace ductility demands of Structure S1 under the FOE- and MCE-level ground motions, respectively. At the MCE level, the designed Frame S1 well satisfies the collapse prevention targets. The peak demand of interstory drift ratio and brace ductility is approximately 3.7% and 11.3, respectively, both of which are noticeably less than the targets. This implies sufficient safety margin in the SMABF. It is also worth noting the performance of the code-based frame, in which the interstory drift ratio in the top story violates the deformation limit, which may lead to severe damage or collapse in this story. Considering the brace ductility demand is 12, Cu-Al-Mn [20], FeNCATB [43], and mono-crystalline Cu-Al-Be [18] are possible candidates to be used in the SMAB. The first story still presents the minimum geometric mean response, whereas the other stories exhibit quite uniform response. At the FOE level, the designed Structure S1 slightly exceeds the performance targets in terms of inter-story drift ratios, because it is directly designed at the DBE level, that is, the design base shear is determined based on the DBE spectrum. In this example, the performance targets at the FOE level are more critical than those at the other levels. Thus, this result clearly indicates that the design of seismic-resisting structures may not always be governed by the performance targets under significant earthquakes. If a significant exceedance of the performance targets is observed, then the structural design should

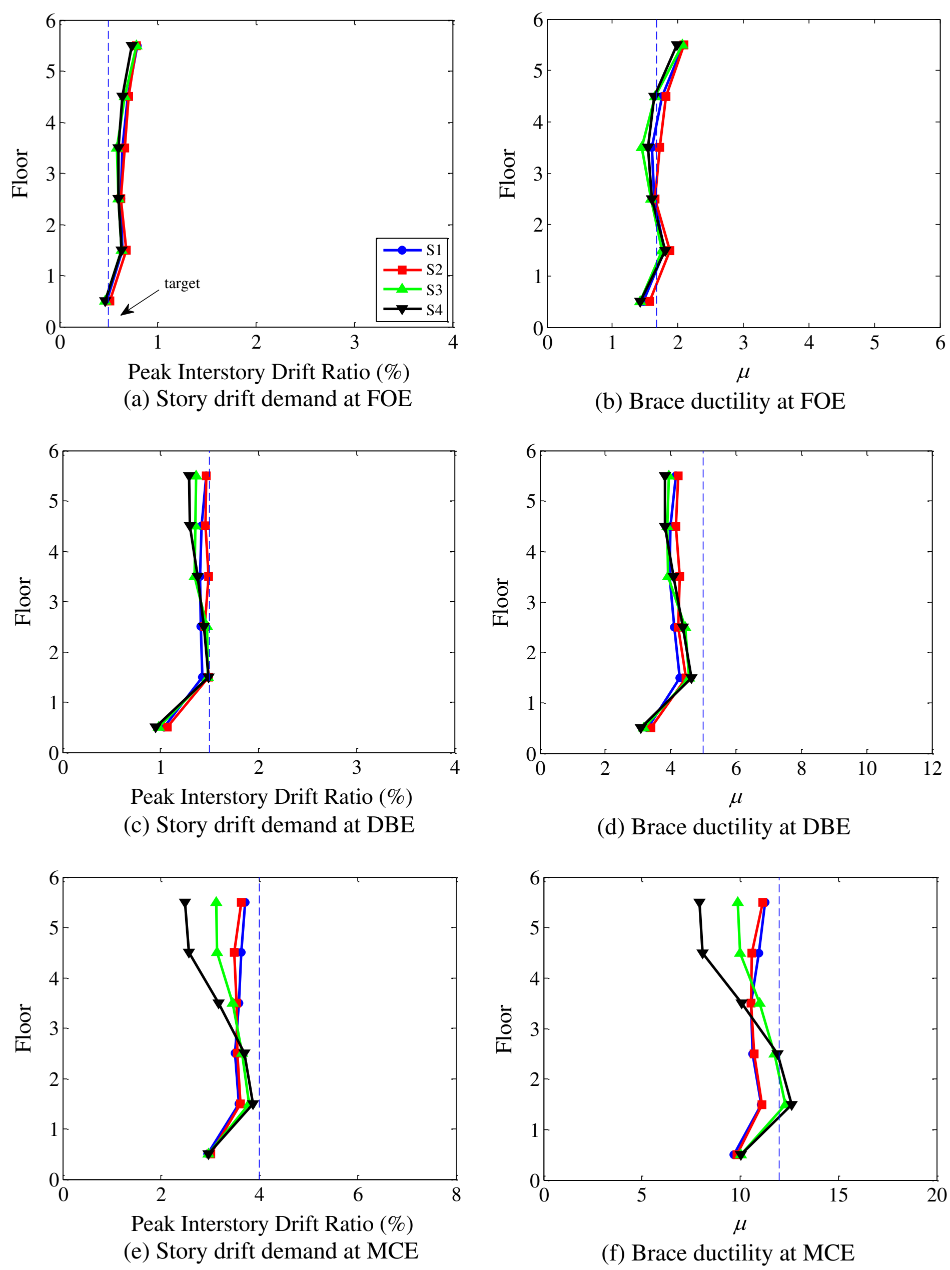

Fig. 12. Seismic performances of the four designed frames with various hysteretic parameters of SMABs.

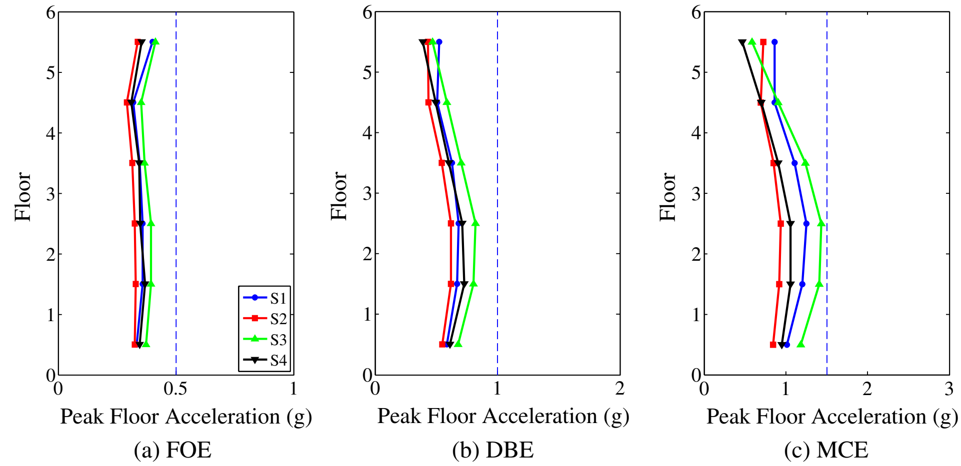

Fig. 13. Peak floor acceleration along the building height at three seismic hazard levels.

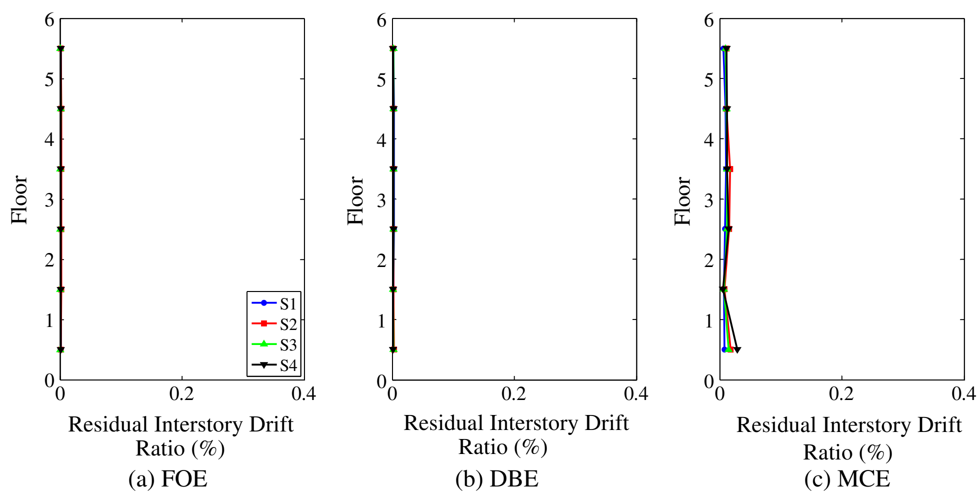

Fig. 14. Residual inter-story drift ratio along the building height at three seismic hazard levels.

be adjusted or the structure should be redesigned according to the most stringent performance targets (i.e., the FOE-level performance targets in this case). However, no further adjustment to the design is made in this study given that the inter-story drift ratios slightly exceed the targets by less than 0.3% and brace ductility demand still reasonably satisfies the performance targets. The ductility demands in some FOE-level cases are approximately a unit, which implies that those braces are fully elastic. Fig. 12 compares the seismic performance of the four designed frames (S1–S4) in terms of peak inter-story drift ratios and peak ductility demands. The performance targets at the three seismic hazard levels are also illustrated in the figure. All four frames are designed to satisfy the same performance targets despite the different design base shears used in each frame. In general, all the structures perform similarly and satisfy design targets, except for slight exceedances of the prescribed targets at the FOE level. This result validates the efficacy of the proposed PBSD method, which can design the SMABFs by considering different hysteretic parameters to achieve the same seismic performance.

Fig. 13 examines peak floor acceleration demand at the FOE, DBE, and MCE levels. Floor acceleration demands are satisfactorily controlled and are less than the performance targets in all four structures at the three seismic hazard levels. The distribution of peak floor accelerations is fairly uniform along the building height. In general, the four design frames exhibit similar seismic performances with regard to peak acceleration demands. Structure S2 gives the best control performance at the three seismic levels because its braces are designed with enhanced α and β values.

Fig. 14 shows the residual inter-story drift ratios of the four designed frames after FOE, DBE, and MCE earthquakes. The residual inter-story drift ratios are nearly zero at the FOE and DBE levels, and remain very small even at the MCE level. The residual inter-story drift ratio tends to concentrate in the first story because of the yielding of the fixed column bases. No plastic hinge is formed in the beam and column sections except for the fixed column bases. The residual deformation in the upper stories is attributed to the unrecovered plastic rotation at the column bases. The geometric mean residual inter-story drift ratio is less than 0.03% at the MCE level, which is considerably less than the peak inter-story drift ratios. The inelastic deformation is nearly completely recovered because of the excellent SC capacity of SMABs.

Fig. 15 plots the most critical points in terms of the P–M interactions at the column bases, where the horizontal and vertical axes represent the normalized bending moment and axial load, respectively. Since the bending moment dominates the deformation, these critical points occur when the bending moments reach their

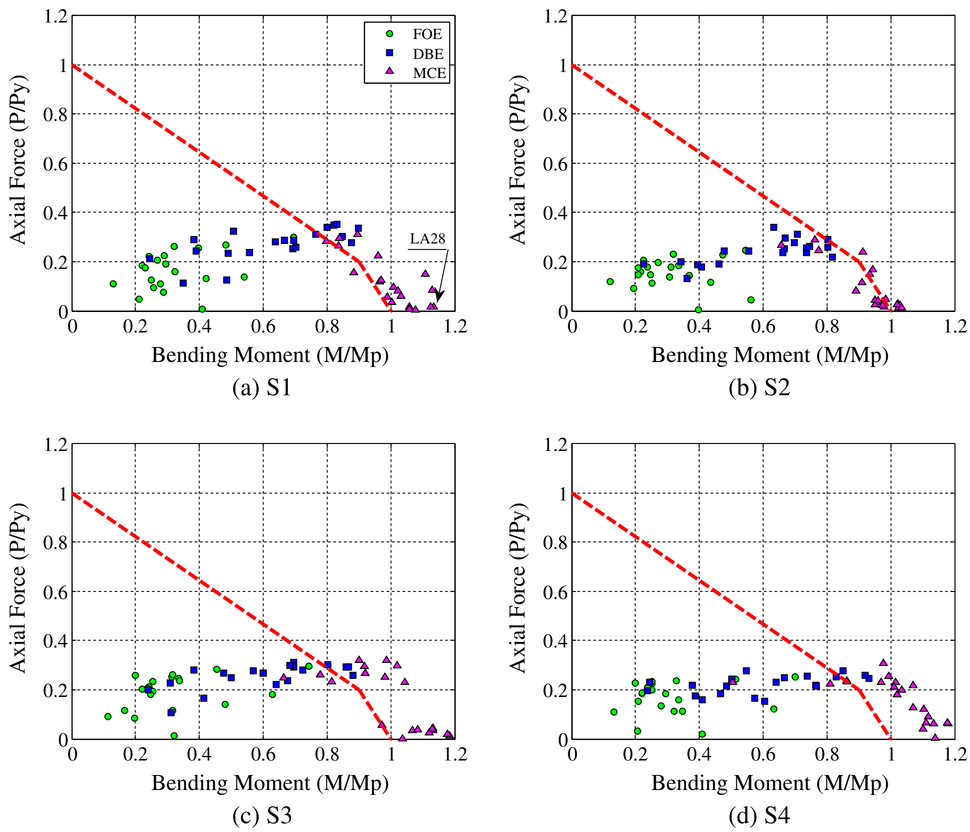

Fig. 15. The most critical P-M interactions at the column bases at three seismic hazard levels.

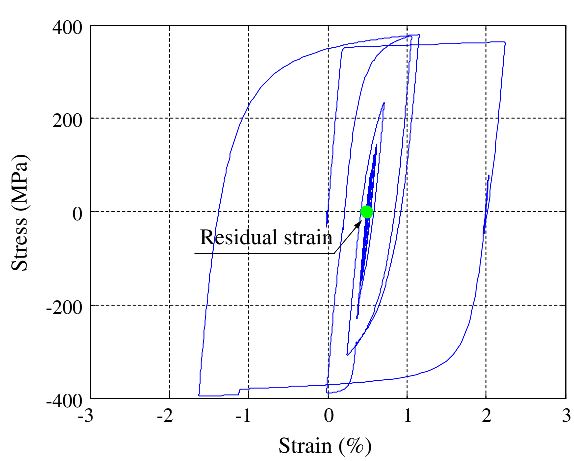

Fig. 16. Stress-strain of the outermost fiber at column base section of Structural S1 under ground motion LA28.

peak values. All points are assembled in the first quadrant for easy comparison. The four frames (S1-S4) have no plastic hinge under all ground motions at the FOE level and most ground motions at the DBE levels. As ground motion intensity increases, plastic hinges form in several cases at the DBE level and more so at the MCE level. A similar trend is observed in all four structures. Although the formed plastic hinges produce inelastic deformation demand, residual deformation remains minimal because of the SC capability of SMABs. This can be illustrated by the stress–strain curve of the outermost fiber at the column base section shown in Fig. 16, which corresponds to the selected seismic response of Structure S1 under the ground motion record LA 28.

6. Conclusions

This study investigates the seismic design of SC steel frames with SMABs. The novel seismic-resisting bracing elements using superelastic SMAs exhibit favorable SC and energy-dissipation capabilities. Based on the performance-based plastic design, this study develops a PBSD approach for SMABFs with the following particular modifications: (1) the μ-R-T relationship of SDOF systems with FS models is determined through regression analysis and used in PBSD; (2) two important hysteretic parameters, namely, the "post-yield" stiffness ratio and the energy dissipation factor, are explicitly considered in PBSD to account for the great variability in these two hysteretic parameters; and (3) a modified lateral force pattern is used in PBSD to mitigate the noticeable high-mode effect that was highlighted in previous seismic analyses of SMABFs. To validate the developed PBSD approach, four examples of six-story seismic-resisting SMABFs are designed with different combinations of "post-yield" stiffness ratio (α) and hysteresis width (β). The four frames are initially designed according to the prescribed performance targets at the DBE level, whereas the seismic performances of the designed frames at three seismic hazard levels (i.e., FOE, DBE, and MCE) are assessed through nonlinear time-history analyses after the design process.

The results of the nonlinear time-history analyses successfully validate the developed PBSD approach for SMABFs. Some notable observations are as follows:

1. despite their different designs, the four SMABFs associated with different hysteretic parameters can satisfactorily achieve the same performance targets prescribed in advance
2. the final designs of the four SMABFs reveal that greater α and/or β parameters of braces are favorable in terms of cost-effectiveness;

3. the modified lateral force pattern adopted in PBSD can successfully mitigate the high-mode effect in seismic responses; as a result, the designed SMABFs exhibit uniform height-wise distribution of peak inter-story drift ratios, even if the frames exhibit inelastic behavior during severe earthquakes; and
4. the properly designed SMABFs exhibit limited structural damage and permanent deformation even after very strong earthquakes, which clearly demonstrates the superior seismic performance of this emerging type of SC seismic-resisting structural systems.

SMABs are assumed to be applied in an indoor environment with relatively stable room temperature. Identifying SMA materials that are suitable for outdoor applications with great temperature variation and subsequently developing a corresponding design approach to take into account the temperature impact needs to be conducted in future studies.

Acknowledgments

The authors are grateful for the financial support from the National Natural Science Foundation of China (Project No. NSFC-51208447), The Hong Kong Polytechnic University (Project No. 4-ZZCG), Chinese National Engineering Centre for Steel Construction (Hong Kong Branch), and the Fundamental Research Funds of Shandong University. The findings and opinions expressed in this paper are solely those of the authors and not necessarily the views of the sponsors.

References

[1] Rosenblueth E, Meli R. The 1985 Mexico earthquake: causes and effects in Mexico City. Concr Int (ACI) 1986;8(5):23–34.
[2] McCormick J, Aburano H, Ikenaga M, Nakashima M. Permissible residual deformation levels for building structures considering both safety and human elements. In: Proceedings of the 14th world conference on earthquake engineering, Beijing. China; 2008. Paper No. 05-06-0071.
[3] Priestley MJ, Macrase G. Seismic tests of precast beam-to-column joint subassemblages with unbonded tendons. PCI J 1996;41(1):64–81.
[4] Ricles JM, Sause R, Garlock MM, Zhao C. Post-tensioned seismic resistant connections for steel frames. J Struct Eng 2001;127(2):113–21.
[5] Christopoulos C, Filiatrault A, Uang CM, Folz B. Post-tensioned energy dissipating connections for moment resisting steel frames. J Struct Eng 2002;128(9):1111–20.
[6] Garlock M, Ricles J, Sause R. Experimental studies on full-scale post-tensioned steel connections. J Struct Eng 2005;131(3):438–48.
[7] Christopoulos C, Tremblay R, Kim HJ, Lacerte M. Self-centering energy dissipative bracing system for the seismic resistance of structures: development and validation. J Struct Eng 2008;134(1):96–107.
[8] Clayton P, Berman J, Lowes L. Seismic design and performance of self-centering steel plate shear walls. J Struct Eng 2012;138(1):22–30.
[9] Erochko J, Christopoulos C, Tremblay R, Kim HJ. Shake table testing and numerical simulation of a self-centering energy dissipative braced frame. Earthq Eng Struct Dyn 2013;42(11):1617–35.
[10] Eatherton MR, Ma X, Krawinkler H, Deierlein GG, Hajjar JF. Quasi-static cyclic behavior of controlled rocking steel frames. J Struct Eng 2014;140(11).
[11] Chou CC, Tsai WJ, Chung PT. Development and validation tests of a dual-core self-centering sandwiched buckling-restrained brace (sc-sbrb) for seismic resistance. Eng Struct 2016;121:30–41.
[12] Dowden DM, Purba R, Bruneau M. Behavior of self-centering steel plate shear walls and design considerations. J Struct Eng 2011;138(1):11–21.
[13] Xu LH, Fan XW, Li ZX. Development and experimental verification of a pre-pressed spring self-centering energy dissipation brace. Eng Struct 2016:49–61.
[14] Dolce M, Cardone D. Mechanical behaviour of shape memory alloys for seismic applications 2. Austenite NiTi wires subjected to tension. Int J Mech Sci 2001;43(11):2657–77.
[15] DesRoches R, McCormick J, Delemont M. Cyclic properties of superelastic shape memory alloy wires and bars. J Struct Eng 2004;130(1):38–46.
[16] Zhu S, Zhang Y. A thermomechanical constitutive model for superelastic SMA wire with strain-rate dependence. Smart Mater Struct 2007:1696–707.
[17] Zhang Y, Camilleri JA, Zhu S. Mechanical properties of superelastic Cu-Al-Be wires at cold temperatures for the seismic protection of bridges. Smart Mater Struct 2008;17:025008. 9pp.
[18] Qiu CX, Zhu S. Characterization of cyclic properties of superelastic monocrystalline Cu–Al–Be SMA wires for seismic applications. Constr Build Mater 2014;72:219–30.
[19] Zhang Y, Zhu S. Seismic response control of building structures with superelastic shape memory alloy wire dameprs. ASCE J Eng Mech 2008;134(3):240–51.
[20] Araki Y, Endo T, Omori T, Sutou Y, Koetaka Y, Kainuma R, Ishida K. Potential of superelastic Cu–Al–Mn alloy bars for seismic applications. Earthq Eng Struct Dynam 2011;40(1):107–15.
[21] Wilde K, Gardoni P, Fujino Y. Base isolation system with shape memory alloy device for elevated highway bridges. Eng Struct 2000;22(3):222–9.
[22] Dolce M, Cardone D, Marnetto R. Implementation and testing of passive control devices based on shape memory alloys. Earthq Eng Struct Dynam 2000;29(7):945–68.
[23] Dolce M, Cardone D, Ponzo FC, Valente C. Shaking table tests on reinforced concrete frames without and with passive control systems. Earthq Eng Struct Dynam 2005;34(14):1687–717.
[24] McCormick J, DesRoches R, Fugazza D, Auricchio F. Seismic assessment of concentrically braced steel frames with shape memory alloy braces. J Struct Eng 2007;133(6):862–70.
[25] Zhu S, Zhang Y. Seismic analysis of concentrically braced frame systems with self-centering friction damping braces. J Struct Eng 2008;134(1):121–31.
[26] Zhu S, Zhang Y. Seismic behavior of self-centring braced frame buildings with reusable hysteretic damping brace. Earthq Eng Struct Dyn 2007;36:1329–46.
[27] Andrawes B, DesRoches R. Effect of hysteretic properties of superelastic shape memory alloys on the seismic performance of structures. Struct Control Health Monit 2007;14(2):301–20.
[28] Sharabash AM, Andrawes BO. Application of shape memory alloy dampers in the seismic control of cable-stayed bridges. Eng Struct 2009;31(2):607–16.
[29] Zhu S, Zhang Y. Loading rate effect on superelastic SMA-based seismic response modification devices. Earthq Struct 2013;4(6):607–27.
[30] Alam MS, Youssef MA, Nehdi M. Analytical prediction of the seismic behavior of superelastic shape memory alloy reinforced concrete elements. Eng Struct 2008;30:3399–411.
[31] Ozbulut OE, Hurlebaus S. Optimal design of superelastic-friction base isolators for seismic protection of highway bridges against near-field earthquakes. Earthq Eng Struct Dyn 2011;40:273–91.
[32] Shrestha KC, Araki Y, Nagae T, et al. Effectiveness of superelastic bars for seismic rehabilitation of clay-unit masonry walls. Earthq Eng Struct Dyn 2013;42:725–41.
[33] Zhu S, Qiu CX. Incremental dynamic analysis of highway bridges with novel shape memory alloy isolators. Adv Struct Eng 2014;17(3):429–38.
[34] Fang C, Yam MCH, Lam ACC, Zhang YY. Feasibility study of shape memory alloy ring spring systems for self-centring seismic resisting devices. Smart Mater Struct 2015;24(7):75024–42.
[35] Fang C, Yam MCH, Lam ACC, Xie LK. Cyclic performance of extended end-plate connections equipped with shape memory alloy bolts. J Constr Steel Res 2014;94:122–36.
[36] Xu X, Zhang Y, Luo Y. Self-centering modularized link beams with post-tensioned shape memory alloy rods. Eng Struct 2016;112:47–59.
[37] Qiu C, Zhu S. Shake table test and numerical study of self-centering steel frame with SMA braces. Earthq Eng Struct Dyn 2016. doi: http://dx.doi.org/10.1002/eqe.2777.
[38] Kim HJ, Christopoulos C. Seismic design procedure and seismic response of post-tensioned self-centering steel frames. Earthq Eng Struct Dyn 2009;38(3):355–76.
[39] Priestley MJN, Kowalsky MJ. Direct displacement-based seismic design of concrete buildings. Bull New Zeal Soc Earthq Eng 2000;33(4):421–44.
[40] O'Reilly GJ, Goggins J, Mahin SA. Performance-based design of a self-centering concentrically braced frame using the direct displacement-based design procedure.15 WCEE, Lisboa; 2012.
[41] Eatherton MR, Ma X, Krawinkler H, Mar D, Billington S, Hajjar JF, Deierlein GG. Design concepts for controlled rocking of self-centering steel-braced frames. J Struct Eng 2014;140(11):04014082.
[42] Leelataviwat S, Goel SC, Stojadinovic B. Toward performance-based seismic design of structures. Earthq Spectra 1999;15(3):435–61.
[43] Tanaka Y, Himuro Y, Kainuma R, Sutou Y, Omori T, Ishida K. Ferrous polycrystalline shape-memory alloy showing huge superelasticity. Science 2010;327:1488–90.
[44] Sommerville P, et al. Development of ground motion time histories for Phase 2 of the FEAM/SAC steel project. SAC background document SAC/BD-91/04, SAC joint venture, Sacramento, Calif; 1997.
[45] Seo CY. Influence of ground motion characteristics and structural parameters on seismic responses of SDOF systems Ph.D. dissertation. Bethlehem (PA): Department of Civil and Environmental Engineering, Lehigh University; 2005.
[46] Housner GW. Limit design of structures to resist earthquakes. Proceedings of the world conference on earthquake engineering 1956;5:1–11.
[47] Lee SS, Goel SC, Chao SH. Performance-based seismic design of steel moment frames using target drift and yield mechanism. In: 13th world conference on earthquake engineering. BC (Canada): Vancouver; 2004. p. 1–6.
[48] Deierlein GG, Krawinkler H, Cornell CA. A framework for performance-based earthquake engineering. In: Pacific conference on earthquake engineering. p. 1–8.
[49] Chao SH, Goel SC. A seismic design method for steel concentric braced frames (CBF) for enhanced performance. In: Proc., 4th int. conf. on earthquake engineering. Taipei, Taiwan.

[50] Chao SH, Goel SC. Performance-based seismic design of eccentrically braced frames using target drift and yield mechanism as performance criteria. AISC Eng J 2006;43(3):173–200.
[51] Goel SC, Chao SH. Performance-based plastic design of special truss moment frames. AISC Eng J 2008;45(2):127–50.
[52] Sahoo DR, Chao SH. Performance-based plastic design method for buckling-restrained frames. Eng Struct 2010;32:2950–8.
[53] Yang TY, Li YJ, Leelataviwat S. Performance-based design and optimization of buckling restrained knee braced truss moment frame. J Perform Constr Facil 2014;28:A4014007. SPECIAL ISSUE: Performance of Timber and Hybrid Structures.
[54] Akiyama H. Earthquake-resistant limit-state design of buildings. Japan: University of Tokyo Press; 1985.
[55] Chopra AK. Dynamics of structures: theory and applications to earthquake engineering. Upper Saddle River (NJ, USA): Prentice Hall Inc.; 2001.
[56] American Society of Civil Engineers (ASCE). Minimum design loads for buildings and other structures. Reston (VA); 2010.
[57] Qiu CX, Zhu S. High-mode effects on seismic performance of multi-story self-centering braced steel frames. J Constr Steel Res 2016;119:133–43.
[58] Chao SH, Goel SC, Lee SS. A seismic design lateral force distribution based on inelastic state of structures. Earthq Spectra 2007;23(3):547–69.
[59] AISC. Seismic provisions for structural steel buildings. ANSI/AISC 341-10. Chicago; 2010.
[60] Sabelli R, Mahin SA, Chang C. Seismic demands on steel-braced buildings with buckling-restrained braces. Eng Struct 2003;25:655–66.
[61] FEMA. NEHRP recommended provisions for seismic regulations for new buildings and other structures. Washington (DC): Federal Emergency Management Agency; 1997.
[62] Fahnestock LA, Ricles JM, Sause R. Experimental evaluation of a large-scale buckling-restrained braced frame. J Struct Eng 2007;133(9):1205–14.
[63] American Society of Civil Engineers (ASCE). Seismic Rehabilitation of Existing Buildings (41-06). Reston (VA); 2007.
[64] SEAOC. Performance based seismic engineering of buildings. Vision 2000 report, vols. I and II. Sacramento (California): Structural Engineers Association of California; 1995.
[65] OpenSees. Open system for earthquake engineering simulation (OpenSees), v 2.4.1 [Computer software]. Berkeley (CA): Pacific Earthquake Engineering Research Center; 2013.
[66] Neuenhofer A, Filippou FC. Evaluation of nonlinear frame finite-element models. J Struct Eng 1997;123(7):958–66.